

# End-to-End Intelligent User-Specific Constellation Optimization in PS-32-QAM-based Flexible Coherent PON with Enhanced Sensitivity and Dynamic Range

Sizhe Xing<sup>(1)</sup>, Zhongya Li<sup>(1)</sup>, Guoqiang Li<sup>(1)</sup>, Aolong Sun<sup>(1)</sup>, Jianyang Shi<sup>(1)</sup>, Nan Chi<sup>(1, 2)</sup>, Junwen Zhang<sup>(1, 2)\*</sup>

<sup>(1)</sup> Key Lab of EMW Information (MoE), Fudan University, Shanghai, China, 200433

<sup>(2)</sup> Peng Cheng Lab, Shenzhen 518055, China, [junwenzhang@fudan.edu.cn](mailto:junwenzhang@fudan.edu.cn)

**Abstract** We propose and demonstrate an end-to-end intelligent constellation optimization scheme in PS-QAM-based FLCSPON under user-specific access conditions. With deep-learning-based autoencoder for transmitter, channel, and receiver, results show 3.7-dB power-budget improvement and 6.1-dB dynamic-range enhancement for PS-32-QAM FLCSPON with 250-Gbps peak line-rate after 50-km SMF. ©2023 The Author(s)

## Introduction

Optical access networks or passive-optical network (PON) have experienced significant evolution over the past decades, driven by the ever-increasing demand for high-bandwidth services [1]. In this process, the ITU-T 50G standard has become a reality following the introduction of IEEE's 25/50G NG-EPON [2]. To address the demand for high-speed access and power budget, coherent PON (CPON) technology, thanks to its superior receiver sensitivity performance, high-order modulation and advanced DSP [3], has emerged as a solution for 100G and beyond access. Meanwhile, to meet the demand for flexibility, the rate-adaptive PON, namely, flexible PON (FLCS-PON) has recently been proposed [4]. To combine the advantages of both technologies, a novel approach, FLCSPON, has been proposed [5], [6], which can flexibly provide massive users in a large dynamic range with high speed.

To support the flexibility of the transmitted signal rate, several ways of changing the rates in PON system has been reported, including TFDMA architecture [7], adaptive coded-modulation [6], and probabilistic shaping (PS) [8]. However,

there have been few researches focused on user-specific constellation optimization in FLCSPON considering the dynamic access conditions in terms of different SNR and linear or nonlinear impairments. The natural diversity of user channels in FLCSPON makes it not only necessary but also a logical step to perform end-to-end (E2E) optimizations for different users. In recent years, E2E optimization [9] has gained widespread attention in the field of optical communications due to its ability to optimize the entire system to improve overall performance.

In this work, we propose and demonstrate an end-to-end intelligent user specific constellation optimization scheme for a PS-QAM based FLCSPON system. A deep-learning-based autoencoder is applied for E2E optimization under different SNR and nonlinear access conditions, while considering the optical pass loss (OPL) differences. Our proposed scheme achieves a 6.1 dB improvement in dynamic range and a 3.7 dB enhancement in power-budget for a PS-32QAM-based FLCSPON at 250 Gbps peak line-rate after a 50-km SMF transmission. Additionally, we demonstrate a 413 dB·Gbps dynamic-range and net-rate product (DRNRP) [8]

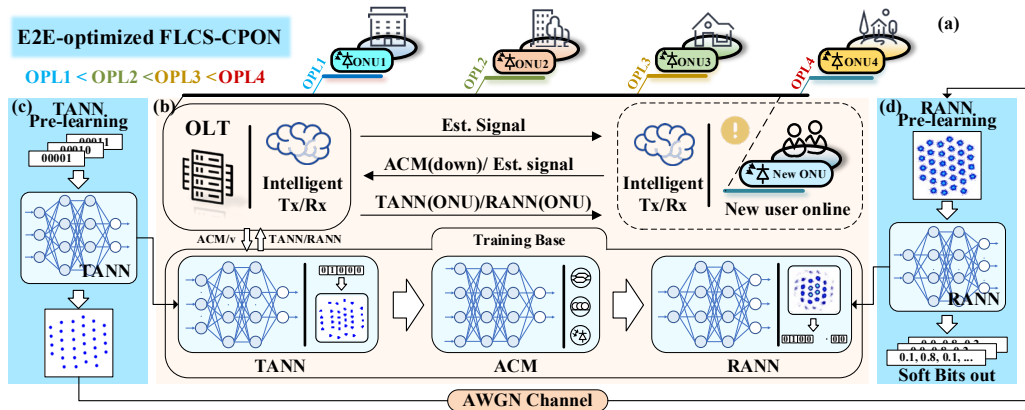


**Fig. 1:** (a) the schematic of a CPON system, (b) the principle of E2E-optimized user-specific rate improvement in FLCSPON, (c) and (d) the pre-training procedure of the T-ANN and R-ANN.

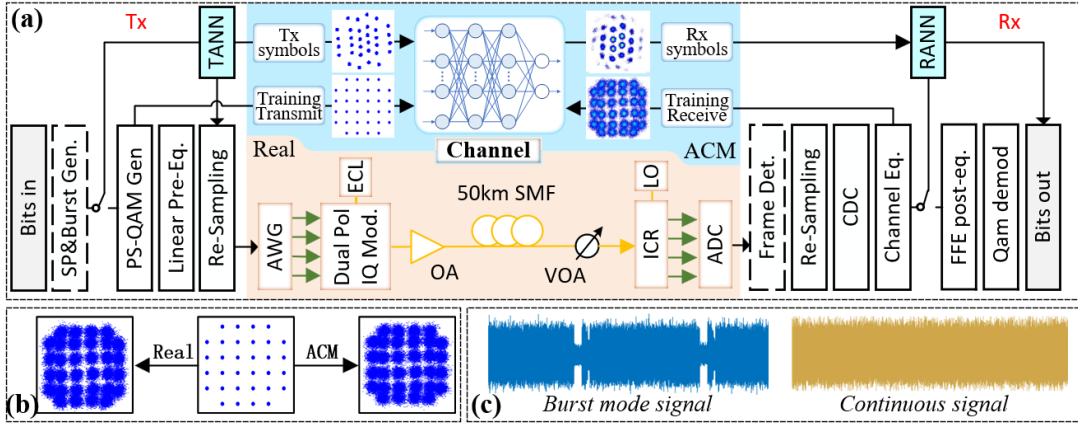


Fig. 2: (a) Schematic of the E2E optimized FLCS-CPON experimental setup, (b) the input and output constellation of real and ACM channel, (c) continuous and burst-mode signals

improvement due to the enhanced sensitivity and dynamic range.

### Principle of E2E Optimization for FLCS-CPON

Fig. 1 shows the principle of E2E-optimized FLCS-CPON, illustrating the cooperation between intelligent autoencoder and the FLCS-CPON system. Fig. 1(a) shows a typical access network with four groups of optical network units (ONUs) that exhibit diverse OPLs to the optical line terminal (OLT). The horizontal thick black line represents the OPL distance, with the left side indicating a smaller OPL. Fig. 1(b) demonstrates how E2E optimization works when a new user goes online. After registration, the OLT will first send an estimation signal to the ONU. At the ONU side, it will establish an Artificial Neural Network-based Channel Model (ACM) to simulate the downstream channel and transmit it along with a new signal series for upstream channel estimation to the OLT. After receiving the new signal series for upstream channel estimation, an upstream ACM can also be established. At the OLT, a proper  $v$  factor for PS-based bitstream generation can be found with the corresponding ACM, and both are then sent to the training base. The training base can train the constellation autoencoder, including the transmitter ANN (T-ANN) and the receiver ANN (R-ANN), based on the input ACM and PS shaping factor  $v$ . When the input is the upstream ACM and shaping factor  $v$ , the T-ANN(ONU) and the R-ANN(OLT) will be obtained. When the input is the downstream ACM and  $v$  value, the T-ANN(OLT) and the R-ANN(ONU) will be obtained. Next, the T-ANN (ONU) and R-ANN (ONU) are transmitted to the ONU side and all the ANNs are deployed in the intelligent Tx/Rx at both ends.

The training base comprises three main blocks: the T-ANN, ACM, and the R-ANN. The T-ANN encodes the transmitted signal from bits to complex symbols. The ACM acts like a real channel, introducing distortion from nonlinearity

distortion inter-symbol interference, and Gaussian noise into the signal from T-ANN. The R-ANN performs post-equalization and QAM demodulation, decoding the distorted 2-dimension symbols into one-hot encoding format.

Fig. 1(c) and 1(d) show the pre-training procedure of the T-ANN and R-ANN respectively, where the ACM is substituted by an AWGN channel model. In order to adjust the constellation distribution output from the T-ANN, an unsupervised learning loss function minmax Euclidean distance (MMED) is introduced, aiming to maximize the Euclidean distance between each symbol, which can be calculated as:

$$L_{MMED} = \frac{\min[d_{i,j}]}{\sqrt{\frac{\sum x_n^2}{N}}} + \frac{\left| \frac{\sum x_n}{N} \right|}{\sqrt{\frac{\sum x_n^2}{N}}} + \left( \sqrt{\frac{\sum x_n^2}{N}} - 1 \right)^2 \quad (1)$$

Where  $d_{i,j}$ ,  $x_n$  and  $N$  represents the distance between the  $i$  and  $j$ -th symbol, the  $n$ -th received symbol, and the total number of the sequence.

### Experimental Setup and Results

Fig. 2 (a) shows the experimental setup of the E2E-optimized FLCS-CPON system, including DSP flows for both burst mode and continuous mode. The setup of traditional CPON system and its DSP are presented at the bottom of Fig. 2(a), where two additional steps dedicated to burst mode operation are highlighted with dashed boxes. And the burst mode signal and continuous signal are shown in Fig. 2 (c). To generate a burst mode frame, a few sync patterns (SPs) are added at the transmitter, and at the beginning of the receiver DSP, a frame detection process is performed. Despite these two steps, the signal is resampled to the AWG matched sample rate before PS-QAM generation and linear pre-equalization. Resampling, chromatic dispersion compensation (CDC), MIMO channel equalization, and additional FFE are crucial steps to recover the received signal to bits again.

The transmitted signal is converted into an electrical signal by the 120-GSa/s AWG and

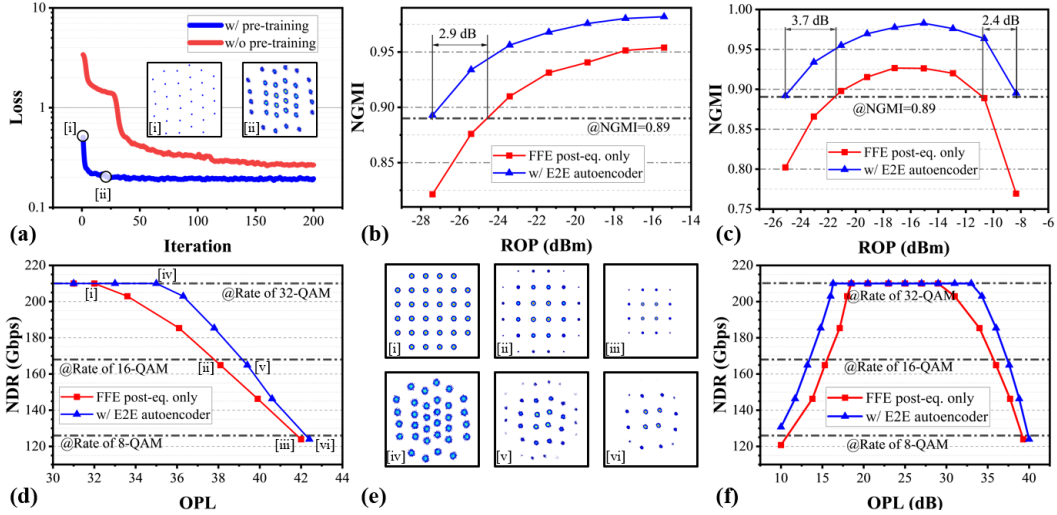


**Fig. 3:** (a) the learning curve with or without pre-training, (b) sensitivity in continuous mode, (c) dynamic range in burst mode, (d) NDR in continuous mode and six typical constellations in (e), (f) NDR in burst mode.

modulated onto the light by the dual-pol. IQ modulator. The optical signal is amplified by an optical amplifier (OA) and transmitted over a 50 km optical fiber. At the receiver side, a variable optical attenuator (VOA) is used for sensitivity test. The received signal is then mixed with the LO and sampled to a 128Gsa/s electrical signal by the real-time oscilloscope.

The simulated ACM utilizes the signals generated from PS-QAM modulation and channel equalization as the transmitted and received signals. Fig. 2(b) compares the constellations after the ACM and the real channel, demonstrating that the ACM finely model the real channel. The E2E optimized autoencoder is then generated, the T-ANN generates the transmitted symbols with constellation optimized while the R-ANN will demodulate them to bits after channel equalization.

To verify the efficiency of the pre-training, the learning curve with or without pre-training are compared in Fig. 3(a), which highlights the advantage of pre-training in achieving faster convergence to lower loss. In our system, a NGMI threshold of 0.89 is used as with 0.84 overall coding rate [10]. In Fig. 3(b) and 3(c), the performance of the autoencoder-aided 32-QAM is illustrated in both continuous and burst modes. In continuous mode, the sensitivity of 32-QAM signal is improved by 2.9 dB for the autoencoder in comparison with Rx-side FFE-only case. And in the burst-mode the sensitivity is improved by 2.4 dB for the autoencoder compared with Rx-side FFE-only case, while the total dynamic range is further extended by 6.1 dB to 16.8 dB when considering the improved performance at the low-OPL range. Fig. 3(d) shows the gain in net-data-rates (NDR) brought by the autoencoder as the OPL increases in continuous mode. Fig. 3(e) illustrates the 32 QAM constellations using

regular Gray coding (i-iii) and E2E optimized autoencoder (iv-vi) at different PS shaping factors. In the burst-mode, dynamic range and NDR are estimated in Fig. 3(f). Table 1 summarizes the dynamic range and power budget of FLCSPON system using Rx-side FFE only and E2E optimized autoencoder at different net-data-rates. By using the autoencoder, a 413 dB·Gbps improvement in DRNRP [8] is achieved, thanks the improved sensitivity and dynamic range.

## Conclusions

An end-to-end intelligent user specific constellation auto-optimization scheme in PS-

**Tab. 1:** performance comparison of FFE only and autoencoder at different net-data-rates

Net-data-rate	Methods	Dynamic Range(dB)	Power Budget(dB)
210 Gbps	FFE only	10.7	29.4
	Autoencoder	16.8	33.1
168 Gbps	FFE only	20.1	35.6
	Autoencoder	23.9	37.3
126 Gbps	FFE only	28.9	39.3
	Autoencoder	30	40.0

QAM based FLCSPON system is proposed and demonstrated in this work. The deep-learning based E2E autoencoder improves the dynamic range and the power budget by 6.1 dB and 3.7 dB, respectively, for PS-QAM-based FLCSPON at 250Gbps line rate over 50-km SMF. Additional 413 dB·Gbps improvement in DRNRP is also demonstrated.

## Acknowledgements

This work was supported in part by the National Natural Science Foundation of China under Grants 62171137, 62235005 and 61925104, in part by the Natural Science Foundation of Shanghai under Grant 21ZR1408700, and in part by the Major Key Project of PCL.

## References

- [1] J. Kani, S. Kaneko, K. Hara, and T. Yoshida, "Optical Access Network Evolution for Future Super-Broadband Services and 6G Mobile Networks", in 2021 European Conference on Optical Communication (ECOC), Sep. 2021, pp. 1–4. DOI: [10.1109/ECOC52684.2021.9606132](https://doi.org/10.1109/ECOC52684.2021.9606132).
- [2] J. Zhang and Z. Jia, "Coherent Passive Optical Networks for 100G/λ-and-Beyond Fiber Access: Recent Progress and Outlook", IEEE Network, vol. 36, no. 2, Art. no. 2, Mar. 2022, DOI: [10.1109/MNET.005.2100604](https://doi.org/10.1109/MNET.005.2100604).
- [3] M. S. Faruk, X. Li, D. Nasset, I. N. Cano, A. Rafel, and S. J. Savory, "Coherent Passive Optical Networks: Why, When, and How", IEEE Communications Magazine, vol. 59, no. 12, pp. 112–117, Dec. 2021, DOI: [10.1109/MCOM.010.2100503](https://doi.org/10.1109/MCOM.010.2100503).
- [4] R. Borkowski, Y. Lefevre, A. Mahadevan, D. van Veen, M. Straub, R. Kaptur, B. Czerwinski, B. Cornaglia, V. Houtsma, W. Coomans, R. Bonk, and J. Maes, "FLCS-PON—an opportunistic 100 Gbit/s flexible PON prototype with probabilistic shaping and soft-input FEC: operator trial and ODN case studies", Journal of Optical Communications and Networking, vol. 14, no. 6, Art. no. 6, Jun. 2022, DOI: [10.1364/JOCN.452036](https://doi.org/10.1364/JOCN.452036).
- [5] S. Xing, G. Li, J. Chen, J. Zhang, N. Chi, Z. He, and S. Yu, "First Demonstration of PS-QAM based Flexible Coherent PON in Burst-Mode with 300G Peak-Rate and Record Dynamic-Range and Net-Rate Product up to 7,104 dB·Gbps", in 2022 Optical Fiber Communications Conference and Exhibition (OFC), Mar. 2022, pp. 1–3.
- [6] M. Xu, H. Zhang, Z. Jia, and L. A. Campos, "Adaptive Modulation and Coding Scheme in Coherent PON for Enhanced Capacity and Rural Coverage", in Optical Fiber Communication Conference (OFC) 2021, Washington, DC: OSA, 2021, p. Th5I.4. DOI: [10.1364/OFC.2021.Th5I.4](https://doi.org/10.1364/OFC.2021.Th5I.4).
- [7] J. Zhang, Z. Jia, H. Zhang, M. Xu, J. Zhu, and L. Alberto, "Rate-Flexible Single-Wavelength TFDm 100G Coherent PON based on Digital Subcarrier Multiplexing Technology", in Optical Fiber Communication Conference (OFC) 2020, San Diego, California: OSA, 2020, p. W1E.5. DOI: [10.1364/OFC.2020.W1E.5](https://doi.org/10.1364/OFC.2020.W1E.5).
- [8] S. Xing, G. Li, A. Sun, J. Chen, Z. He, J. Zhang, and N. Chi, "Demonstration of PS-QAM Based Flexible Coherent PON in Burst-Mode With 300G Peak Rate and Ultra-Wide Dynamic Range", J. Lightwave Technol., vol. 41, no. 4, pp. 1230–1239, Feb. 2023, DOI: [10.1109/JLT.2022.3208575](https://doi.org/10.1109/JLT.2022.3208575).
- [9] B. Karanov, M. Chagnon, F. Thouin, T. A. Eriksson, H. Bulow, D. Lavery, P. Bayvel, and L. Schmalen, "End-to-End Deep Learning of Optical Fiber Communications", J. Lightwave Technol., vol. 36, no. 20, pp. 4843–4855, Oct. 2018, DOI: [10.1109/JLT.2018.2865109](https://doi.org/10.1109/JLT.2018.2865109).
- [10] R. Zhang, N. Kaneda, Y. Lefevre, A. Mahadevan, D. van Veen, and V. Houtsma, "Probabilistic and Geometric Shaping for Next-Generation 100G Flexible PON", in 2020 European Conference on Optical Communications (ECOC), Brussels, Belgium: IEEE, Dec. 2020, pp. 1–4. DOI: [10.1109/ECOC48923.2020.9333172](https://doi.org/10.1109/ECOC48923.2020.9333172).